

Absorption and scattering of massless scalar waves by Frolov black holes

Jining Tang^{1,*} Yang Huang^{2,†} and Hongsheng Zhang^{2‡}

School of Physics and Technology, University of Jinan,

336 West Road of Nan Xinzhuang, Jinan, Shandong 250022, China

Abstract

We comprehensively investigate the absorption and scattering of massless scalar waves by Frolov black holes, which is a class of regularization of the Reissner–Nordström spacetime. By analyzing the null geodesics, we determine the photon sphere radius and the critical impact parameter, deriving the geometric capture cross section and the classical differential scattering cross section. Utilizing the partial-wave method, we numerically compute the absorption and scattering cross sections across a broad frequency range. Our numerical results show excellent agreement with the low-frequency limit and the high-frequency sinc approximation, as well as with the semiclassical glory approximation. We analyze the dependence of the spectra on the charge and the regularization parameter (Hubble length). Under the horizon-radius normalization, we observe that the total absorption cross section increases with the regularization parameter, a behavior we attribute to the variation of the dimensionless mass. Furthermore, by comparing Frolov, Reissner–Nordström, and Hayward black holes, we demonstrate that their absorption and scattering patterns are nearly indistinguishable when their critical impact parameters or glory impact parameters are matched. This indicates that the photon sphere geometry predominantly governs scalar field interactions, while the detailed core structure plays a secondary role. Our work underscores the potential of wave-based probes to test regular black hole geometries and their observable imprints.

Keywords: Regular black holes, Massless scalar wave, Scattering, Absorption

*Electronic address: aishiker1998@gmail.com

†Electronic address: sps_Huangy@ujn.edu.cn

‡Electronic address: sps_zhanghs@ujn.edu.cn (corresponding author)

I. INTRODUCTION

With the advent of gravitational-wave astronomy and black hole imaging[1–6], understanding the interaction between waves and black holes has become more crucial than ever. The scattering and absorption of fields by black holes provide powerful probes of spacetime structure and tests of general relativity[7, 8]. Related wave-scattering phenomena have also been discussed in alternative gravitational settings, e.g., for (quasi-)spherical gravitational waves scattered from black strings in massive gravity[9]. Propagating fields leave characteristic imprints in their absorption and differential scattering cross sections, which depend both on universal near-horizon physics and on the detailed geometry of the photon sphere and its unstable null orbits. At low frequencies these observables typically display universal behaviour, largely insensitive to the fine details of the spacetime [10], whereas at high frequencies they are controlled by the capture properties of null geodesics and by the structure of the photon sphere, which also underlies the phenomenology of black hole shadows and photon rings as observed in M87* and Sgr A* [11, 12]. Wave-optics diffraction phenomena can also arise in black-hole scattering, such as the PoissonArago spot discussed for gravitational waves[13].

For a minimally coupled massless scalar field, this picture is well understood in benchmark geometries. In the zero-frequency limit the total absorption cross section approaches the area of the event horizon [14, 15], while in the high-frequency regime it oscillates around the geometric capture cross section, with an oscillatory pattern that can be related to the properties of the unstable photon orbit and the associated Regge poles of the scattering matrix [16, 17]. These features have been established in detail for Schwarzschild and Reissner–Nordström black holes through a combination of partial-wave analysis and explicit geodesic control [18, 19]. Full-wave computations of scalar scattering in nontrivial charged backgrounds, together with comparisons to geodesic and Regge-pole/glory approximations, have been carried out for charged dilatonic black holes [20].

The quest to resolve the central singularities predicted by general relativity has motivated the study of regular black holes (RBHs) [21–24]. Many such solutions arise in nonlinear electrodynamics and modify the inner structure while preserving asymptotic flatness [25–27]. In particular, the Bardeen and Hayward spacetimes [28, 29] provide simple models in which regular cores and effective charges reshape the effective potential and photon-sphere data, leading to characteristic changes in greybody factors and large-angle scattering patterns [30, 31].

As a charged generalization of the Hayward solution, the Frolov black hole [32] has recently

attracted considerable interest. Its thermodynamic properties, quasinormal modes and shadows have been investigated in a variety of contexts [33–35]. However, to the best of our knowledge, a systematic study of massless-scalar absorption and scattering in this spacetime, covering analytic low- and high-frequency limits and full-frequency numerical results, is still lacking.

Against this backdrop, the present work develops a comprehensive analysis of massless scalar absorption and scattering by Frolov black holes. At the classical level we study null geodesics, identifying the photon sphere and the associated critical impact parameters, and we derive the weak-deflection and backward glory approximations for the differential cross section. Within the partial-wave formalism we obtain the radial equation and its effective potential, and we derive the usual low-frequency limit and a high-frequency sinc approximation expressed in terms of the critical impact parameter and Lyapunov exponent. We then compute the absorption and differential scattering cross sections numerically over a broad frequency range, comparing them with the analytic approximations and exploring how the two Frolov parameters jointly affect the spectra. In particular, we examine cases in which different parameter choices yield very similar absorption and scattering patterns, and relate this behaviour to the structure of the effective potential and the underlying geodesics.

The remainder of this paper is organized as follows. In Sec. II we review the Frolov spacetime, analyse null geodesics and discuss the corresponding classical capture and scattering properties. In Sec. III we present the partial-wave formalism for a massless scalar field, derive the effective potential, and obtain the analytic low- and high-frequency limits for the absorption and scattering cross sections. Sec. IV is devoted to the numerical results: we summarize our normalization choices, describe the numerical implementation, and present the full-frequency absorption and scattering spectra for a range of Frolov parameters, including comparisons with Reissner–Nordström and Hayward black holes at matched impact parameters. We conclude our results in Sec. V. Throughout this work we use natural units with $G = c = \hbar = 1$ and metric signature $(-, +, +, +)$. For analytic expressions we keep the mass parameter M explicit to facilitate comparison with the existing literature, whereas in our numerical calculations and plots we adopt the horizon-radius normalization $r_h = 1$, defined by $f(r_h) = 0$.

II. CLASSICAL ANALYSIS

We consider the Frolov BH, which is a static regular black hole, whose line element is given by [32]

$$ds^2 = -f(r)dt^2 + \frac{1}{f(r)}dr^2 + r^2(d\theta^2 + \sin^2\theta d\phi^2), \quad (1)$$

where

$$f(r) = 1 - \frac{r^2(2Mr - Q^2)}{r^4 + (2Mr + Q^2)\alpha^2}. \quad (2)$$

Here M and Q respectively denote the mass and charge parameter of the black hole. The regularized parameter α represents the Hubble length, which is related to the effective cosmological constant $\Lambda_{\text{eff}} = 3/\alpha^2$, characterize the curvature core of the Frolov BH. For keeping the event horizon surviving, the Hubble length is bounded with $\alpha \leq \sqrt{16/27}M$.

As $r \rightarrow \infty$, the spacetime is asymptotically Reissner–Nordström $f(r) \approx f_{\text{RN}}(r) = 1 - \frac{2M}{r} + \frac{Q^2}{r^2}$, where near the center $r \rightarrow 0$ the expansion $f(r) = 1 - \frac{\Lambda_{\text{eff}}}{3}r^2 + \dots$ signals regularity.

A. Null geodesics and geometrical limits

The classical Lagrangian related to the null geodesic trajectory is given by

$$\mathcal{L} = \frac{1}{2}g_{\mu\nu}\frac{dx^\mu}{d\lambda}\frac{dx^\nu}{d\lambda} = 0. \quad (3)$$

Let us constrain the motion of particles on the equatorial plane without loss of generality, the equation above gives

$$f(r)\dot{t}^2 - \frac{\dot{r}^2}{f(r)} - r^2\dot{\phi}^2 = 0. \quad (4)$$

It's clear that there exist two conserved quantities

$$E = \frac{\partial \mathcal{L}}{\partial \dot{t}} = -f\dot{t} \quad , \quad L = -\frac{\partial \mathcal{L}}{\partial \dot{\phi}} = r^2\dot{\phi}, \quad (5)$$

where E and L are respectively the energy and the angular momentum of the massless particle. Then the geodesic equation can be written as

$$\dot{r}^2 = f^2\dot{t}^2 - fr\dot{\phi}^2 = E^2 - f\frac{L^2}{r^2}, \quad (6)$$

here we can write the equation of motion Eq.(6) in the form

$$\dot{r}^2 + V_{\text{eff}} = E^2 \quad (7)$$

by defining

$$V_{\text{eff}} = f(r) \frac{L^2}{r^2} = \left[1 - \frac{r^2(2Mr - Q^2)}{r^4 + (2Mr + Q^2)\alpha^2} \right] \frac{L^2}{r^2} \quad (8)$$

In Fig.2, we display the effective potential for massless particles in Frolov BHs with different parameters for illustration.

After using the impact parameter $b \equiv L/E$ as the ratio of angular momentum and energy, we can obtain the orbit equation

$$\left(\frac{dr}{d\phi} \right)^2 = \frac{\dot{r}^2}{\dot{\phi}^2} = r^4 \left(\frac{1}{b^2} - \frac{f}{r^2} \right). \quad (9)$$

It is convenient to introduce $u \equiv 1/r$, the orbit equation can be written as

$$\left(\frac{du}{d\phi} \right)^2 = \left(\frac{du}{dr} \right)^2 \left(\frac{dr}{d\phi} \right)^2 = \mathcal{U}(u) = \frac{1}{b^2} - u^2 f, \quad (10)$$

where $f = f(1/u)$. By differentiating Eq.(10), we get

$$\frac{d^2u}{d\phi^2} = -\frac{u^2}{2} \frac{df}{du} - u f \quad (11)$$

For the Frolov spacetime,

$$f(r) = 1 - \frac{(2Mr - Q^2)r^2}{r^4 + (2Mr + Q^2)\alpha^2}, \quad (12)$$

two orbit equations read

$$\left(\frac{du}{d\phi} \right)^2 = \frac{1}{b^2} - u^2 + \frac{u^3 (2M - Q^2 u)}{\alpha^2 u^3 (2M + Q^2 u) + 1}, \quad (13)$$

$$\frac{d^2u}{d\phi^2} = -\frac{P(u)}{B(u)^2}, \quad (14)$$

where

$$B(u) = 1 + \alpha^2 u^3 (2M + Q^2 u), \quad (15)$$

$$\begin{aligned} P(u) = u & \left[1 - 3Mu + 2Q^2 u^2 + 4\alpha^2 M u^3 + 2\alpha^2 Q^2 u^4 + 2\alpha^2 M Q^2 u^5 \right. \\ & \left. + \alpha^4 (4M^2 u^6 + 4M Q^2 u^7 + Q^4 u^8) \right]. \end{aligned} \quad (16)$$

It is obvious that, for the curvature-free case ($\alpha = 0$),

$$f = 1 - \frac{2M}{r} + \frac{Q^2}{r^2} = 1 - 2Mu + Q^2u^2, \quad (17)$$

the equations are consistent with previous work on RN BHs [19, 36]

$$\left(\frac{du}{d\phi}\right)^2 = \frac{1}{b^2} - u^2 + 2Mu^3 - Q^2u^4, \quad (18)$$

$$\frac{d^2u}{d\phi^2} = -u + 3Mu^2 - 2Q^2u^3. \quad (19)$$

From the orbit equation Eq.(10), one sees $\mathcal{U}(u) \geq 0$ along the orbit. There is a critical value of the impact parameter b_c , which related to the critical radius r_c of the unstable circular orbit, namely

$$b_c = \frac{L_c}{E_c} = \frac{r_c}{\sqrt{f(r_c)}}, \quad 2f(r_c) - r_c \frac{df(r_c)}{dr} = 0. \quad (20)$$

The trajectories can be obtained by numerically solving the orbit equation (9). In Fig.1, we give the null geodesic orbits in Frolov spacetime with several parameters. In particular, the photon-sphere data entering b_c also control the CAM ingredients, like Regge frequency and damping, as explicitly demonstrated in Ref. [37].

These null-geodesic quantities, in particular the photon-sphere radius and the critical impact parameter b_c , also underlie the optical appearance of compact objects. Recent analyses of photon dynamics and shadows in rotating spacetimes with parity-odd hair provide closely related geodesic diagnostics [38]. See also Ref. [39] for a systematic discussion of null-particle dynamics and shadows in a general rotating black-hole geometry. Light rings and lensing diagnostics are not restricted to black holes; for related discussions in rotating boson-star spacetimes with parity-odd features, see Ref. [40].

Equation (20) partitions incoming null geodesics into two classes: for $|b| < b_c$ the trajectory crosses the potential barrier and is captured, whereas for $|b| > b_c$ it turns back to infinity. The geometric cross section, which is the classical capture cross section of geodesics, is well known[41]

$$\sigma_{\text{geo}} = \pi b_c^2. \quad (21)$$

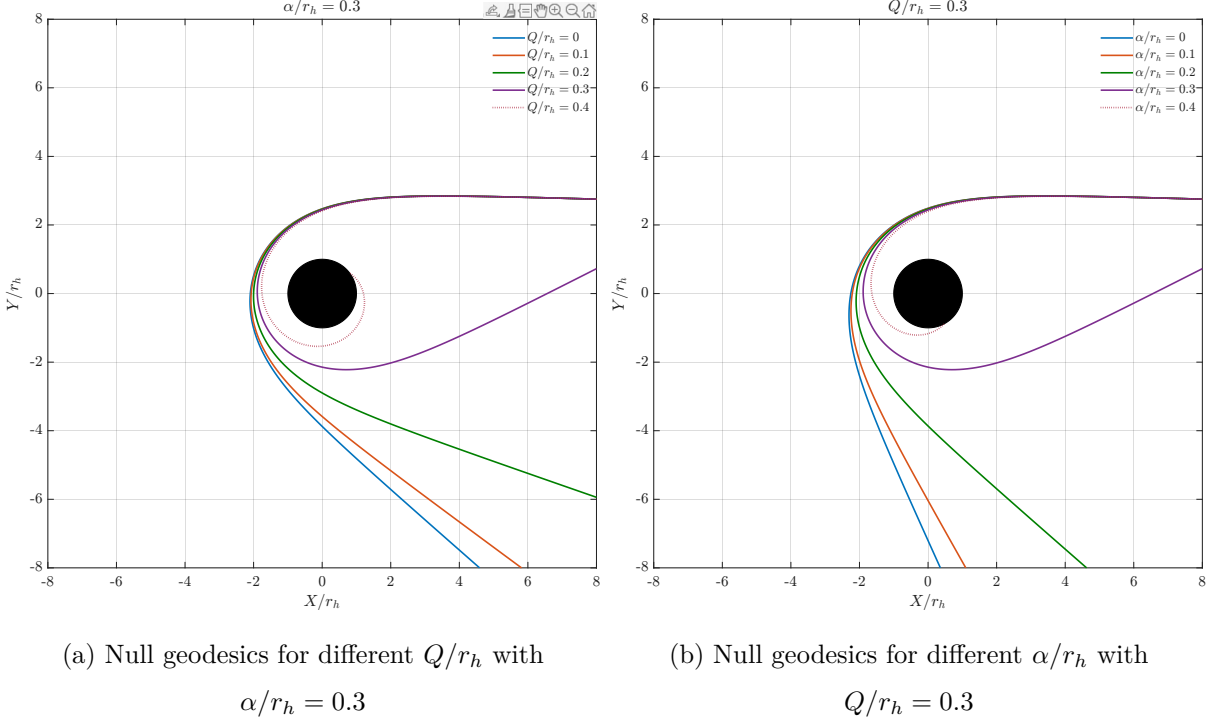
In high frequency limit, the absorption cross section can be written as the sinc approximation, which involves leading term σ_{geo} and the oscillatory correction[16, 17]

$$\sigma_{\text{abs}}^{\text{hf}} \approx \sigma_{\text{geo}} \left[1 - 8\pi \frac{\Lambda_c}{\Omega_c} e^{-\pi\Lambda_c/\Omega_c} \text{sinc}(2\pi b_c \omega) \right], \quad (22)$$

where $\text{sinc}(x) \equiv \sin(x)/x$. And the photon-sphere angular frequency and Lyapunov exponent[42], $\Omega_c = 1/b_c$ is the angular frequency of the unstable photon circular orbit at r_c . Lyapunov exponent of these circular null geodesics is given by[42]

$$\Omega_c = \frac{1}{b_c} = \frac{\sqrt{f(r_c)}}{r_c}, \quad \Lambda_c = \sqrt{\left. \frac{L^2}{2t^2} V''(r) \right|_{r_c}} = \sqrt{\frac{f(r_c) [2f(r_c) - r_c^2 f''(r_c)]}{2r_c^2}}, \quad (23)$$

will anchor the oscillatory pattern of the high-frequency absorption in Sec. IV B.



(a) Null geodesics for different Q/r_h with $\alpha/r_h = 0.3$

(b) Null geodesics for different α/r_h with $Q/r_h = 0.3$

FIG. 1: Null geodesics for massless particles in the background of Frolov BHs with different values of Q and α for a fixed $b = 3r_h$. The trajectories can be derived numerically by orbit equation Eq. (10). We have set the initial condition r_{inf} at $100r_h$.

B. Weak deflection and Classical scattering

Having established the geometrical-optics limit via the photon sphere (r_c, b_c) and the capture cross section σ_{geo} in the previous subsection, we now focus on the rays that return to infinity, i.e. the scattering branch $b > b_c$. In the scattering case, the deflection angle can be obtained by integrating Eq.(10)

$$\Theta(b) = 2 \int_0^{u_0} \frac{du}{\sqrt{\mathcal{U}(u)}} - \pi = 2 \int_0^{u_0} du \left(\frac{1}{b^2} - u^2 f \right)^{-1/2} - \pi. \quad (24)$$

In the weak-field limit, the deflection angle can be expanded in power of b^{-1}

$$\Theta \approx \frac{4M}{b} + \frac{3\pi}{4b^2} (5M^2 - Q^2) + \mathcal{O}\left(\frac{1}{b}\right)^3, \quad (25)$$

which coincides with the RN result. Expanding the lapse at large radii yields

$$f(r) = 1 - \frac{2M}{r} + \frac{Q^2}{r^2} + \alpha^2 \left(\frac{4M^2}{r^4} - \frac{Q^4}{r^6} \right) + \dots, \quad (26)$$

so the α -dependent corrections start at $\mathcal{O}(r^{-4})$ and therefore enter the weak-deflection series only at $\mathcal{O}(b^{-4})$. This is consistent with the weak-deflection expansion obtained via the Gauss-Bonnet approach in Ref. [35] and with the Hayward case [43].

The classical differential cross section is given by [8]

$$\left. \frac{d\sigma_{\text{sc}}}{d\Omega} \right|_{\text{cl}} = \frac{b}{\sin \theta} \left| \frac{db}{d\theta} \right|. \quad (27)$$

From Eq.(25) and (27), we conclude that the classical differential scattering cross section for small scattering angles is

$$\left. \frac{d\sigma_{\text{sc}}}{d\Omega} \right|_{\text{cl}} = \frac{16M^2}{\Theta^4} + \frac{15\pi M^2}{4\Theta^3} - \frac{3\pi Q^2}{4\Theta^3} + \mathcal{O}\left(\frac{1}{\Theta}\right)^2. \quad (28)$$

It is obvious that the Hubble length α has no effect on the dominant term of classical differential scattering cross section.

For the glory approximation of the scalar scattering cross sections, the backward glory is defined by $\Theta(b_g) = \pi$, in the spacetime of a static and symmetric BH, the glory approximation of the scalar scattering cross sections is [44]

$$\left. \frac{d\sigma_{\text{sc}}}{d\Omega} \right|_{\theta \approx \pi} \approx 2\pi\omega b_g^2 \left| \frac{db}{d\theta} \right|_{\theta=\pi} [J_0(\omega b_g \sin \theta)]^2, \quad (29)$$

where ω is the frequency of the scalar wave, b_g is the impact parameter that corresponds to a deflection angle of π , $J_0(x)$ is a Bessel function of the first kind. Imposing the backward-scattering condition $\theta = \pi + 2n\pi$ ($n = 0, 1, 2, \dots$) yields a discrete set of glory impact parameters b_g^n , where n counts the number of windings of the null geodesic around the photon sphere. In practice, the differential cross section near $\theta \simeq \pi$ is dominated by the $n = 0$ branch, while higher-winding contributions are strongly suppressed [31, 45]. Although the semi-classical glory approximation (29) is formally derived for the high-frequency regime, it remains in very good agreement with the numerical results down to intermediate frequencies [19].

III. PARTIAL-WAVE METHOD

A. Massless scalar field

First we consider a minimally coupled massless scalar obeying the Klein-Gordon equation

$$\nabla_\mu \nabla^\mu \Phi = \frac{1}{\sqrt{-g}} \partial_\mu (\sqrt{-g} g^{\mu\nu} \partial_\nu \Phi) = 0. \quad (30)$$

With the standard separation

$$\Phi = \frac{\psi_{\omega l}(r)}{r} Y_{lm}(\theta, \phi) e^{-i\omega t}, \quad (31)$$

the radial function satisfies a RW-type equation in the tortoise coordinate

$$\frac{d^2}{dr_*^2} \psi_{\omega l} + [\omega^2 - V_{\text{eff}}(r)] \psi_{\omega l} = 0, \quad (32)$$

with effective potential

$$V_{\text{eff}}(r) = f(r) \left[\frac{f'(r)}{r} + \frac{l(l+1)}{r^2} \right], \quad (33)$$

where tortoise coordinate r_* is defined as $f(r)dr_* = dr$.

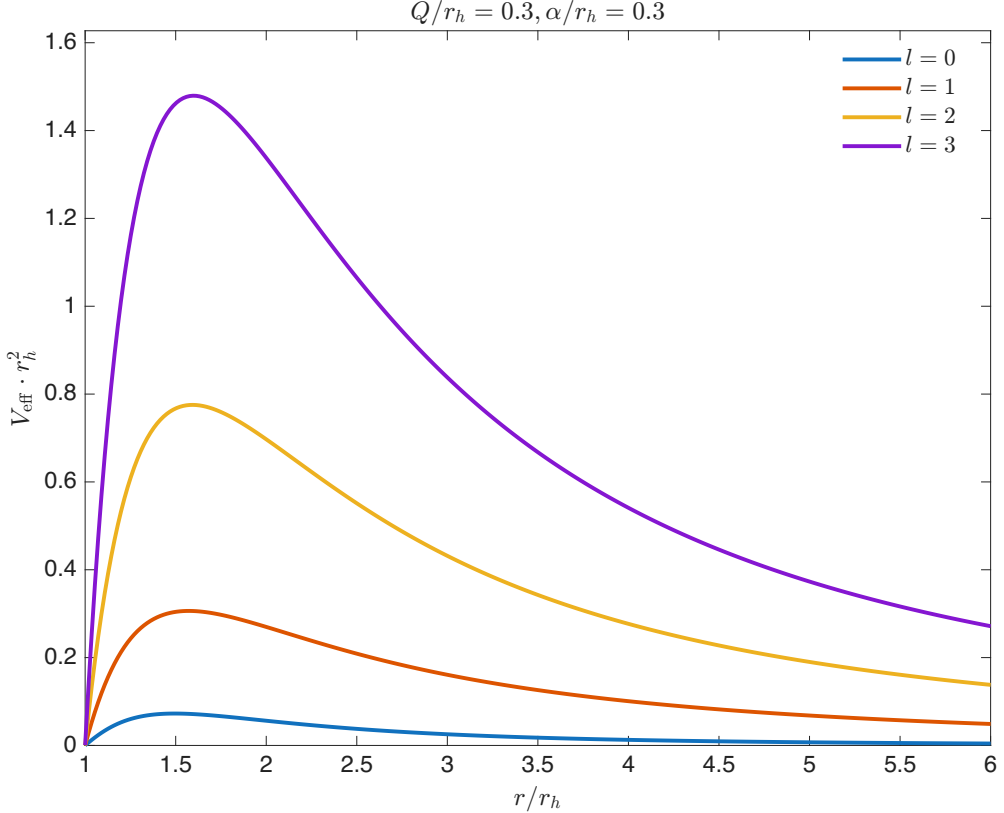


FIG. 2: The effective potential of a Frolov BH with the parameters $Q/r_h = 0.3$ and $\alpha/r_h = 0.3$.

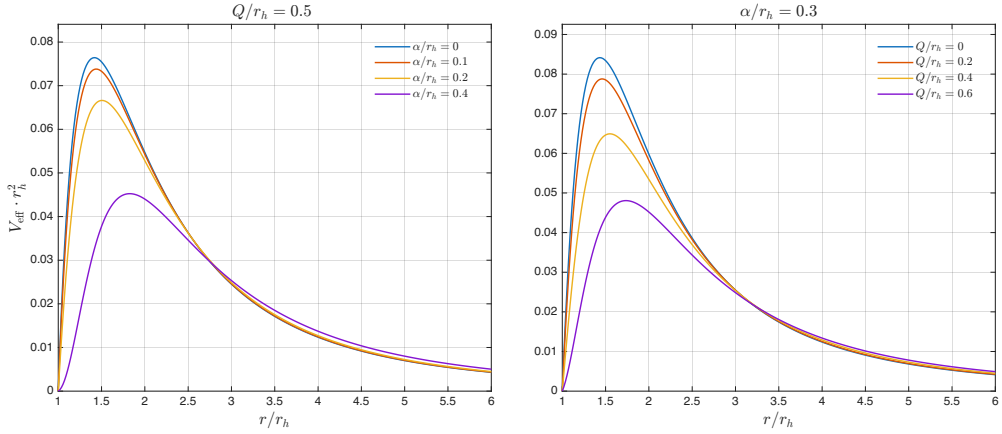


FIG. 3: Effective potential $V_{\text{eff}}(r)$ for the $l = 0$ mode of Frolov BHs.

In Fig. 2 we plot the effective potential for a "mild" Frolov black hole with parameters chosen as $Q/r_h = 0.3$ and $\alpha/r_h = 0.3$. Fig. 3 compares the effective potential, with $l = 0$ for various parameters. As we can see, no matter which parameter is fixed, the maximum of the potential always decreases as the other parameter increases. This apparent discrepancy with the trend reported in works that adopt the $M = 1$ normalization for RN and Hayward black holes arises solely from the different choice of units; a detailed discussion of the relation between the $r_h = 1$ and $M = 1$ conventions is given in Sec. IV.

As $r_* \rightarrow \pm\infty$ the effective potential vanishes, $V_{\text{eff}} \rightarrow 0$, so Eq. (32) reduces to $\psi'' + \omega^2\psi = 0$ and the solutions are plane waves. It is convenient to express the large-argument behavior with the spherical Hankel functions $h_l^{(1)}$ and $h_l^{(2)}$, which satisfy $h_l^{(1)}(z) \sim (-i)^{l+1}e^{iz}/z$ and $h_l^{(2)}(z) \sim i^{l+1}e^{-iz}/z$ as $z \rightarrow \infty$. Imposing purely ingoing behavior at the horizon and an incident-plus-outgoing superposition at infinity yields the boundary conditions

$$\psi_{\omega l} \sim \begin{cases} A_{\omega l}^{\text{tr}} e^{-i\omega r_*}, & r_* \rightarrow -\infty, \\ A_{\omega l}^{\text{in}} e^{-i\omega r_*} + A_{\omega l}^{\text{out}} e^{+i\omega r_*}, & r_* \rightarrow +\infty, \end{cases} \quad (34)$$

and flux conservation gives $|A_{\omega l}^{\text{tr}}|^2 + |A_{\omega l}^{\text{out}}|^2 = |A_{\omega l}^{\text{in}}|^2$.

It is convenient to introduce the partial-wave S -matrix, defined by the ratio of the outgoing and ingoing amplitudes

$$S_l(\omega) = (-1)^{l+1} \frac{A_{\omega l}^{\text{out}}}{A_{\omega l}^{\text{in}}}. \quad (35)$$

The absorption probability of the l -th mode is given by

$$\Gamma_l(\omega) = 1 - |S_l|^2 = \frac{|A_{\omega l}^{\text{tr}}|^2}{|A_{\omega l}^{\text{in}}|^2}, \quad (36)$$

which characterizes the transmission of the scalar wave through the effective potential barrier.

B. Absorption cross sections

The total absorption cross section is the sum over partial contributions

$$\sigma_{\text{abs}} = \sum_{l=0}^{\infty} \sigma_{\text{abs}}^{(l)}, \quad (37)$$

with

$$\sigma_{\text{abs}}^{(l)} = \frac{\pi}{\omega^2} (2l+1) \Gamma_l = \frac{\pi}{\omega^2} (2l+1) \left(1 - \left| \frac{A_{\omega l}^{\text{out}}}{A_{\omega l}^{\text{in}}} \right|^2 \right). \quad (38)$$

In the low-frequency limit only the s-wave survives, then the cross section will approach to the area of BH horizon, this universality first established in Ref. [10] and extended to stationary geometries in Ref. [14]. But in high-frequency regime, capture dominates and the cross section rapidly oscillating around the geometric cross section σ_{geo} , which we have discussed in Sec. II A. Here we give the expression of absorption cross section in two asymptotic limits

$$\sigma_{\text{abs}}^{\text{lf}} \approx A_H, \quad \sigma_{\text{abs}}^{\text{hf}} \approx \pi b_c^2 - 8\pi^2 \frac{\Lambda_c}{\Omega_c^3} e^{-\pi\Lambda_c/\Omega_c} \text{sinc}(2\pi b_c \omega). \quad (39)$$

C. Scattering cross section

The scattering amplitude is given by

$$g(\theta) = \frac{1}{2i\omega} \sum_{l=0}^{\infty} (2l+1) \left[e^{2i\delta_l} - 1 \right] P_l(\cos \theta) \quad (40)$$

and the differential scattering cross section is

$$\frac{d\sigma_{\text{sc}}}{d\Omega} = |g(\theta)|^2, \quad (41)$$

in this description the phase shifts defined in Eq. (35) encode the same information as the classical deflection function discussed in Sec. II.

Our numerical evaluation of $S_l(\omega)$ and the resulting $\sigma_{\text{abs}}(\omega)$ and $d\sigma_{\text{sc}}/d\Omega$, together with comparisons to the low/high-frequency limits and the classical benchmarks of Sec. II, are presented in the next section.

IV. NUMERICAL RESULTS

In this section, we present a series of numerical results concerning the absorption and scattering cross sections of massless scalar field in the background of Frolov spacetimes with variable parameters.

A. Numerical setup

Given the complexity of Frolov black holes, directly solving the horizon by setting the metric function (2) equal to zero would introduce additional computational complexity and numerical uncertainty. For this reason, unlike previous studies on absorption and scattering of BHs, we adopt the normalization by setting $r_h = 1$ instead of working with the commonly used $M = 1$. It is convenient to introduce the normalized parameter

$$q \equiv \frac{Q}{r_h}, \quad \ell \equiv \frac{\alpha}{r_h}, \quad m \equiv \frac{M}{r_h}, \quad (42)$$

in place of the original Q , α and M .

This choice imposes nontrivial constraints on the admissible values of the black hole parameters. The first constraint requires that the charge q satisfy the following inequality with the Hubble length ℓ :

$$q^2 - \ell^4 q^2 + 4\ell^2 q^2 + 3\ell^2 \leq 1. \quad (43)$$

In Fig. 4, we show the parameter space in the (ℓ^2, q^2) plane. The background color encodes the function $E(\ell^2, q^2) = -1 + q^2 - \ell^4 q^2 + \ell^2(3 + 4q^2)$, with the blue region $E \leq 0$ corresponding to configurations that admit an event horizon, while the complementary region $E \geq 0$ represents horizonless geometries. The solid black curve marks the locus $E = 0$, where the two horizons merge and the Frolov BH becomes extremal; its intercepts at $(\ell^2 = 0, q^2 = 1)$ and $(\ell^2 = 1/3, q^2 = 0)$ reproduce, respectively, the extremal Reissner–Nordström and extremal Hayward limits. It is worth noting that, since we employ the horizon radius as our fundamental length scale, the limiting value of the regularizing parameter in the uncharged case is now $\ell = \sqrt{1/3}$, rather than the more familiar $\sqrt{16/27}$ quoted in the $M = 1$ convention.

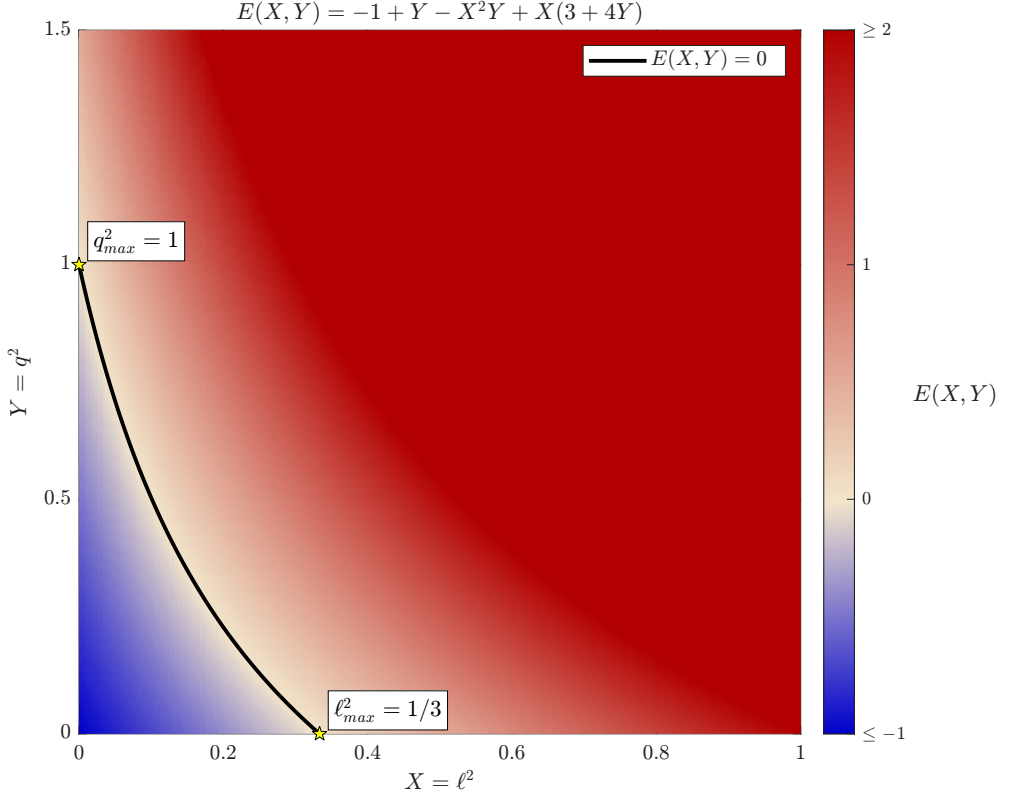


FIG. 4: Parameter space of Frolov BHs in the (ℓ^2, q^2) plane. The blue region corresponds to configurations with an event horizon, and the solid black curve marks the extremal limit.

Within this domain, the condition $f(r_h = 1) = 0$ fixes the dimensionless mass as a function of the remaining parameters

$$m(q, \ell) = \frac{1 + (1 + \ell^2)q^2}{2(1 - \ell^2)}. \quad (44)$$

Figure 5 displays the behaviour of m as a function of q^2 and ℓ^2 within the region of parameter space that admits an event horizon, which we discussed in the last paragraph. One can see that m increases monotonically with both q and ℓ , so different choices of (q, ℓ) along the allowed domain correspond to Frolov BHs of different mass, even though the horizon radius is kept fixed. As a consequence, varying (q, ℓ) at fixed $r_h = 1$ is not directly equivalent to varying the charge Q or the Hubble length α at fixed mass in the usual $M = 1$ normalization. This observation will be important when interpreting, in the next subsections, the dependence of the absorption and scattering cross sections on (q, ℓ) and when comparing our results with previous absorption scattering research in references.

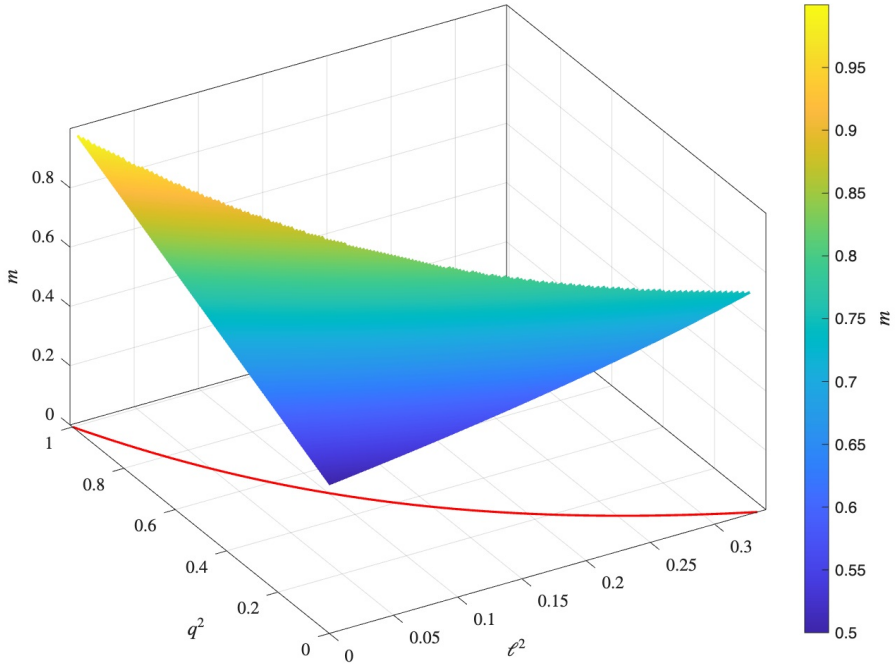


FIG. 5: Normalized mass m of Frolov BHs for a fixed horizon radius $r_h = 1$, restricted to the region admitting an event horizon.

Finally we numerically solve Eq. (32) from the point very close to the event horizon to a region far from the BHs, then match the numerical solutions with the boundary condition given in Eq. (34) to compute the coefficients. In calculations of absorption and scattering cross sections, we perform sums on angular momentum of the scalar wave. For the absorption case, we set $l = 10$, and consider $l = 50$ for the scattering case. To optimize the convergence of the differential scattering cross section at small scattering angles, we employed the well-known YRW method[46, 47]. Related convergence issues of the partial-wave expansion near the optical axis, and a complementary resolution based on finite-radius wavefunctions (avoiding the problematic asymptotic expansion), were analyzed in a rigorous manner in Ref. [48].

B. Scalar absorption

In Fig. 6, we plot the total absorption cross sections (ACS) of massless scalar waves in the Frolov spacetime. The left panel shows the dependence on the Hubble length ℓ for fixed charge Q , whereas the right panel displays the dependence on Q at fixed ℓ , illustrating how the ACS changes

as the parameters are varied toward the extremal regime.

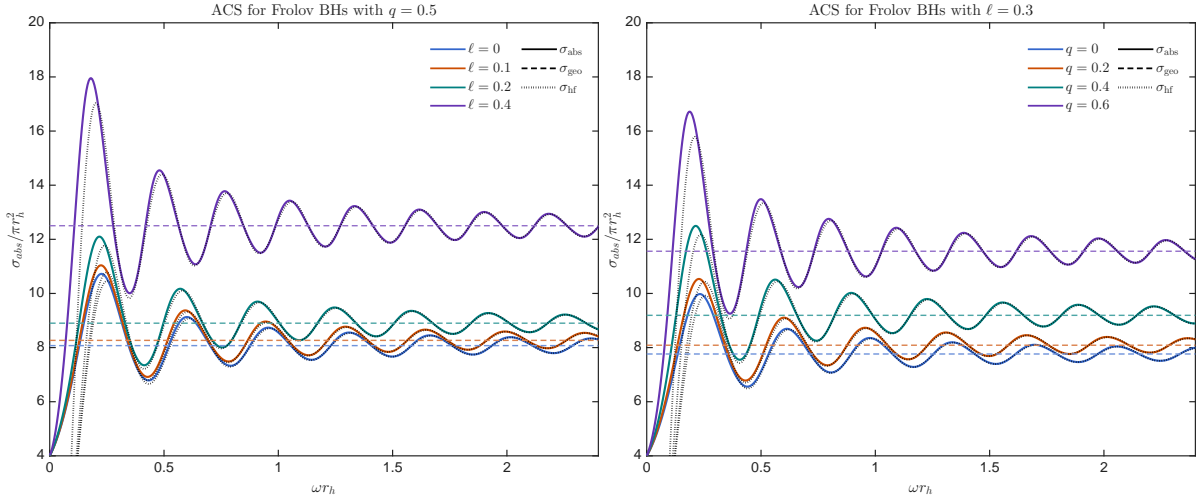


FIG. 6: Total ACS of massless scalar fields in Frolov spacetime. The numerical results (solid lines) are compared with the high-frequency sinc approximation (dotted lines) and the geometric capture limit (dashed lines). Panels display the dependence on the Hubble length ℓ at fixed charge $q = 0.5$ (left) and on q at fixed $\ell = 0.3$ (right)

As we can see in this figure, the numerical results exhibit the expected asymptotic behaviors at both frequency ends. In the low-frequency limit ($\omega r \rightarrow 0$), the cross sections universally converge to the horizon area $\sigma_{\text{abs}} \rightarrow 4\pi r_h^2$, while in the high-frequency regime, the spectra oscillate around the geometric cross section $\sigma_{\text{abs}} \rightarrow \sigma_{\text{geo}} = \pi b_c^2$ with a pattern that is well-described by the semiclassical sinc approximation. Apart from these limits, we observe that the overall amplitude of the ACS typically increases as we increase either q or ℓ . This trend appears opposite to what is reported for RN and Hayward black holes in the standard $M = 1$ normalization, where the total ACS usually decreases as the charge or regularizing parameter grows [19, 43]. However, in our $r_h = 1$ convention the dimensionless mass $m(q, \ell)$ also increases across the allowed parameter space (see Sec. IV and Fig. 5), so part of the apparent growth of the ACS is simply reflecting the change of the overall mass scale rather than a genuine reversal of the underlying geometric effect.

Then we compare the partial ACSs of scalar wave in Frolov spacetime with the same parameters in Fig. 7 as a complementary view of Fig. 6. These plots show explicitly that the parameter dependence of the total ACS is mainly driven by the lowest modes, in particular the s -wave ($l = 0$), while higher- l modes provide comparatively smaller influence.

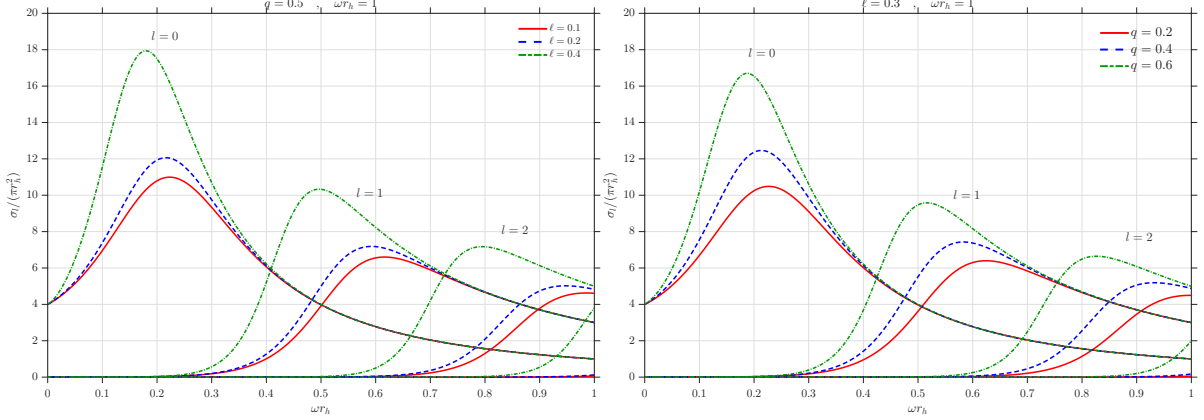


FIG. 7: Partial absorption cross sections of massless scalar waves in the Frolov spacetime for the lowest angular-momentum modes $l = 0, 1, 2$. The left panel shows the dependence on the Hubble length ℓ for fixed charge $Q = 0.5$, whereas the right panel displays the dependence on Q with fixed $\ell = 0.3$.

C. Scattering cross section

In this subsection we discuss the scattering of massless scalar waves by Frolov BHs. The differential scattering cross section is computed from the partial-wave series in Eq. (41), with phase shifts obtained from the numerical integration of the radial equation (32).

First we compare our numerical results for the differential scattering cross sections (DCS) of massless scalar waves in the Frolov spacetime with approximations. It is clearly obtained that the DCS oscillating around the classical DCS, which we have derived in Eq. (28). The pattern agrees well with the classical analytical results in small scattering angle, and is well described by glory approximation(Eq. (29)) in the region $\theta \approx \pi$.

Then Fig. 9 displays the differential scattering cross sections (DCS) for massless scalar waves with frequency $\omega r_h = 3$ in the background of Frolov spacetime, which show the dependency of DCS on the parameters. The left panel shows the effect of varying ℓ at fixed charge, while the right panel shows the effect of varying q at fixed ℓ , where the values chosen are consistent with we used in the absorption work. One can see that the small-angle cross section is much more sensitive to changes in q than to changes in ℓ . The behavior is in agreement with the formula in Eq. (28), where the charge enters the subdominating Θ^{-3} term, whereas the dependence on ℓ appears only through higher-orders corrections that is neglected in the approximation. However at large angles, the effect of ℓ becomes comparable to that of q , which they have a significant effect upon DCS. We also found that the interference fringe width decreases with the increase of two parameters q

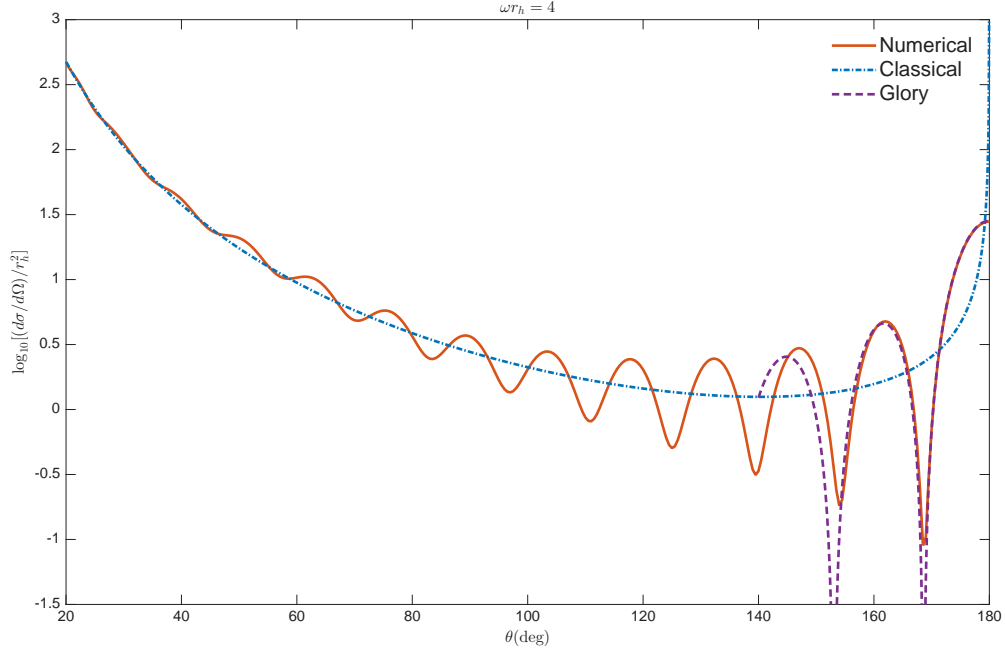


FIG. 8: Comparison between the numerical and the approximate analytical results for the DCS of massless scalar fields in the Frolov spacetime. Here we consider $q = 0.3$ and $\ell = 0.3$ as parameters for frequency $\omega r_h = 4$.

and ℓ for given frequency ωr_h . This behavior is opposite to what is typically found for Reissner–Nordström and Hayward black holes when the mass is kept fixed[19, 43]. This difference arises from our choice of units, where the horizon radius rather than mass is used as the fundamental scale.

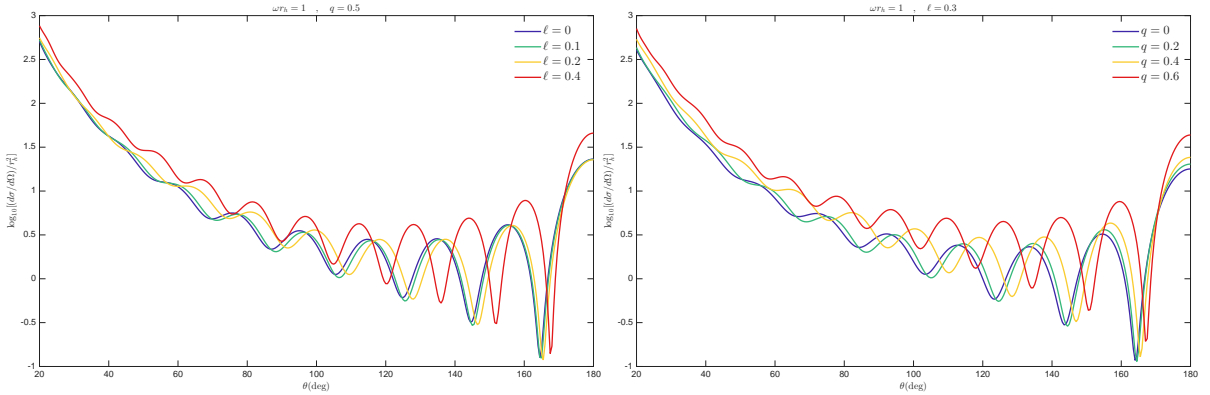


FIG. 9: Differential scattering cross section for Frolov spacetime for different values of q and ℓ , at a representative frequency $\omega r_h = 3$.

D. Similar features for different Frolov BHs

The intriguing work of de Paula et al. [43] investigated under which circumstances the absorption and scattering spectra of Hayward BHs and RN BHs can become almost indistinguishable.

In the absorption problem, they let the critical impact parameters coincide by adjusting appropriate parameters, $b_c^H(\alpha) = b_c^{\text{RN}}(Q)$, and showed that, under this condition, the corresponding total ACS are very similar over the whole frequency range. In the scattering case, they instead matched the impact parameter of the backscattered null geodesics, requiring $b_g^H(\alpha) = b_g^{\text{RN}}(Q)$, and found that the DCS patterns of two black holes are also nearly identical.

Motivated by this observation, we now ask whether a similar correspondence persists when comparing RN, Hayward and Frolov black holes with the same impact parameters. Since the Frolov spacetime reduces to the RN solution and Hayward black hole in appropriate limits, curves of constant impact parameters $b(\ell, q)$ in the (ℓ^2, q^2) plane [cf. Fig. 4] naturally interpolate between these two limiting geometries. Along a given iso- b curve there thus exists a continuous family of Frolov BHs sharing the same impact parameter.

To assess how far the absorption and scattering spectra are influenced by these impact parameters, we focus on the lines with $b_c \simeq 3r_h$ and $b_g \simeq 3r_h$, and select three representative configurations on each line: an Reissner–Nordström black hole, a Hayward black hole and an intermediate Frolov case. As shown in Fig. 10a, we plot the ACSs for three cases with $b_c \simeq 3r_h$ over the whole frequency range. Moreover, Fig. 10b illustrates the comparison between the DCSs in the background of three different spacetimes.

We exhibit, in both panels of Fig. 10, that the ACSs and DCSs for three chosen black hole are basically coincide in the whole frequency/angle range. While the agreement in the asymptotic limits is guaranteed by our parameter matching strategy (fixing r_h for the low-frequency limit and b_c/b_g for the high-frequency limit), the nearly perfect overlap in the intermediate regime is non-trivial. This implies that the iso-spectrality is not merely an artifact of the limits, but stems from the fact that the associated effective potentials possess almost identical barrier shapes around the photon sphere. Consequently, the Frolov, Reissner–Nordström, and Hayward black holes become practically indistinguishable via massless scalar scattering in these configurations.

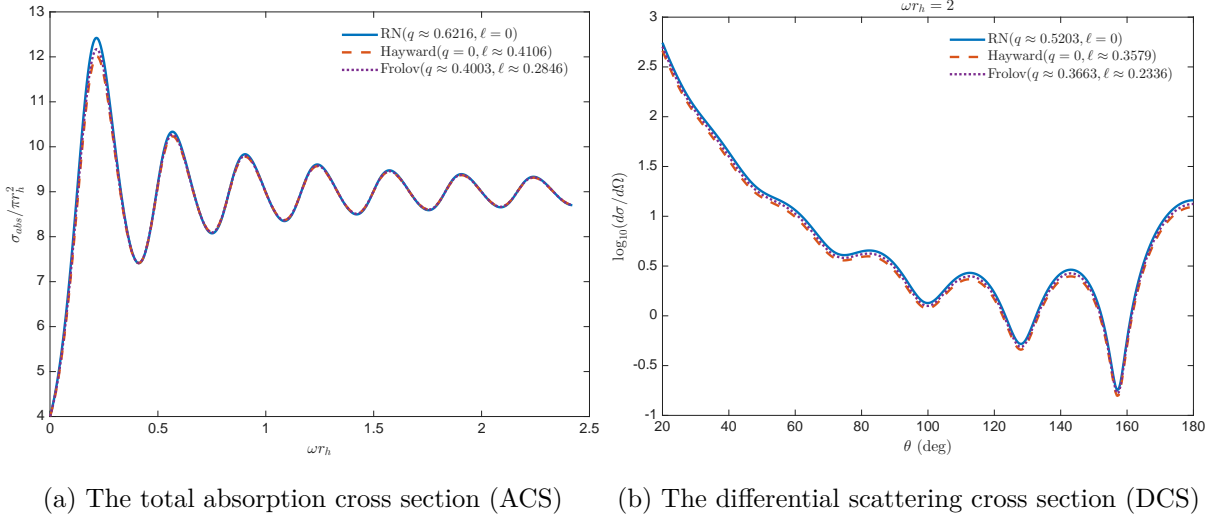


FIG. 10: ACSs and DCSs of Reissner–Nordström, Hayward and Frolov black holes with matched impact parameters. Panel (a) shows configurations with critical impact parameter $b_c \simeq 3 r_h$, whereas panel (b) refers to configurations with glory impact parameter $b_g \simeq 3 r_h$.

V. CONCLUSION

The absorption and scattering of fields by black holes serve as a powerful probe for exploring the fundamental nature of spacetime geometry and horizon structure. Regular black holes, which smooth out central singularities, have been shown to leave distinct signatures in the scalar absorption cross sections and differential scattering cross sections across several specific models[30, 49]. However, a systematic investigation into how the two key parameters of the Frolov spacetime jointly influence these observable quantities over a broad frequency range has remained lacking prior to this work.

In this work, we first conducted a comprehensive null geodesic analysis to confirm the existence of the event horizon in Frolov black holes, pinpoint the location of the photon sphere, and calculate the critical impact parameters that govern the capture process and glory scattering. On the wave physics front, we employed the partial-wave method to investigate minimally coupled massless scalar fields. By solving the radial equation with appropriately imposed boundary conditions, we derived the partial absorption probabilities, total and partial absorption cross sections, as well as the differential scattering cross section. Across the entire parameter space explored, the numerically computed cross sections smoothly bridge the universal low-frequency regime and the high-frequency geometric optics regime, demonstrating excellent agreement with classical approximations and glory approximations within their respective valid domains.

In the numerical analysis we adopted the normalization $r_h = 1$ and mapped the allowed region in the (ℓ^2, q^2) plane where an event horizon exists. In this parametrization the normalized mass m grows monotonically with both q and ℓ , so changing these parameters at fixed r_h does not correspond to the same effect on spacetime as in the more common $M = 1$ convention. This explains why, in our results, the total absorption cross section and the height of the effective potential barrier increase as either parameter is raised, even though related studies of Reissner–Nordström and Hayward black holes at fixed mass report a decreasing trend. The partial–wave decomposition further shows that the lowest mode dominate the low–frequency absorption and drive most of the parameter dependence, while variations of parameters in the scattering problem mainly shift and distort the interference fringe pattern.

Motivated by recent comparisons between different regular metrics at fixed impact parameters, we also examined Frolov, Reissner–Nordström and Hayward black holes chosen to share the same critical impact parameter b_c (for absorption) or glory parameter b_g (for scattering). Along such iso– b_c and iso– b_g curves in parameter space, the effective potentials and the resulting ACS and DCS are found to be very similar. This suggests that, within this class of spacetimes, the dominant features of scalar absorption and scattering are largely controlled by the properties of the unstable photon orbit, while the detailed core structure plays a secondary role.

Several promising directions for extending the present work naturally emerge. First, investigating higher-spin fields or nonminimally coupled scalar fields in the Frolov spacetime would help assess the universality of the patterns identified herein. Second, exploring rotating generalizations of regular black holes could uncover qualitatively new signatures in absorption and scattering, as the interplay between regular cores and frame-dragging effects may introduce novel physical behaviors. Such extensions would further deepen our understanding of the interaction between waves and regular black holes, providing valuable insights for future observational tests of gravitational theories. Beyond the present static setup, it is natural to consider charged/massive scalar probes in charged backgrounds; see, e.g., Ref. [50] and Ref. [51]. It would also be interesting to connect black hole scattering/absorption calculations to wave-optics gravitational-wave lensing, where spin effects can enter naturally [52].

ACKNOWLEDGMENTS

This work is supported by the National Natural Science Foundation of China (NSFC) under Grant nos. 12235019, 12275106 and Shandong Provincial Natural Science Foundation under grant

- [1] Michele Maggiore. *Gravitational waves: Volume 1: Theory and experiments*, volume 1. Oxford university press, 2008.
- [2] Michele Maggiore. *Gravitational Waves: Astrophysics and Cosmology*, volume 2. Oxford University Press, 2008.
- [3] Jolien DE Creighton and Warren G Anderson. *Gravitational-wave physics and astronomy: An introduction to theory, experiment and data analysis*. John Wiley & Sons, 2012.
- [4] Bangalore Suryanarayana Sathyaprakash and Bernard F Schutz. Physics, astrophysics and cosmology with gravitational waves. *Living reviews in relativity*, 12(1):2, 2009.
- [5] Scott A Hughes. Listening to the universe with gravitational-wave astronomy. *Annals of Physics*, 303(1):142–178, 2003.
- [6] Benjamin P Abbott, Richard Abbott, Thomas D Abbott, Matthew R Abernathy, Fausto Acernese, Kendall Ackley, Carl Adams, Thomas Adams, Paolo Addesso, Rana X Adhikari, et al. Observation of gravitational waves from a binary black hole merger. *Physical review letters*, 116(6):061102, 2016.
- [7] Nils Anderson and Bruce Jensen. Scattering by black holes. In *Scattering*, pages 1607–1626. Elsevier, 2002.
- [8] Roger G Newton. *Scattering theory of waves and particles*. Springer Science & Business Media, 2013.
- [9] Hongsheng Zhang and Yang Huang. Spherical gravitational waves and quasi-spherical waves scattered from black string in massive gravity. *Journal of High Energy Physics*, 2021(12):1–11, 2021.
- [10] Sumit R Das, Gary Gibbons, and Samir D Mathur. Universality of low energy absorption cross sections for black holes. *Physical Review Letters*, 78(3):417, 1997.
- [11] Event Horizon Telescope Collaboration. First m87 event horizon telescope results. i. the shadow of the supermassive black hole. *Astrophysical Journal Letters*, 875(1):L1, 2019.
- [12] Event Horizon Telescope Collaboration. First sagittarius a* event horizon telescope results. i. the shadow of the supermassive black hole in the center of the milky way. *Astrophysical Journal Letters*, 930(2):L12, 2022.
- [13] HongSheng Zhang and XiLong Fan. Poisson-arago spot for gravitational waves. *Science China Physics, Mechanics & Astronomy*, 64(12):120462, 2021.
- [14] Atsushi Higuchi. Low-frequency scalar absorption cross sections for stationary black holes. *Classical and Quantum Gravity*, 18(20):L139, 2001.
- [15] Atsushi Higuchi. Addendum to low-frequency scalar absorption cross sections for stationary black holes. *Classical and Quantum Gravity*, 19(3):599, 2002.
- [16] Yves Décanini, Gilles Esposito-Farese, and Antoine Folacci. Universality of high-energy absorption cross sections for black holes. *Physical Review DParticles, Fields, Gravitation, and Cosmology*, 83(4):044032,

2011.

- [17] Norma Sanchez. Absorption and emission spectra of a schwarzschild black hole. *Physical Review D*, 18(4):1030, 1978.
- [18] J A.H. Futterman, F A Handler, and R A Matzner. *Scattering from black holes*. Cambridge University Press, New York, NY, 12 1986.
- [19] Luís CB Crispino, Sam R Dolan, and Ednilton S Oliveira. Scattering of massless scalar waves by reissner-nordström black holes. *Physical Review DParticles, Fields, Gravitation, and Cosmology*, 79(6):064022, 2009.
- [20] Yang Huang and Hongsheng Zhang. Scattering of massless scalar field by charged dilatonic black holes. *The European Physical Journal C*, 80(7):654, 2020.
- [21] Stefano Ansoldi. Spherical black holes with regular center: a review of existing models including a recent realization with gaussian sources. *arXiv preprint arXiv:0802.0330*, 2008.
- [22] Chen Lan, Hao Yang, Yang Guo, and Yan-Gang Miao. Regular black holes: a short topic review. *International Journal of Theoretical Physics*, 62(9):202, 2023.
- [23] KA Bronnikov, H Dehnen, and VN Melnikov. Regular black holes and black universes. *General Relativity and Gravitation*, 39(7):973–987, 2007.
- [24] Cosimo Bambi. *Regular black holes*. Springer, 2023.
- [25] Eloy Ayon-Beato and Alberto Garcia. Regular black hole in general relativity coupled to nonlinear electrodynamics. *Physical review letters*, 80(23):5056, 1998.
- [26] Eloy Ayon-Beato and Alberto Garcia. The bardeen model as a nonlinear magnetic monopole. *Physics Letters B*, 493(1-2):149–152, 2000.
- [27] Leonardo Balart and Elias C Vagenas. Regular black holes with a nonlinear electrodynamics source. *Physical Review D*, 90(12):124045, 2014.
- [28] James Bardeen. Non-singular general relativistic gravitational collapse. In *Proceedings of the 5th International Conference on Gravitation and the Theory of Relativity*, page 87, 1968.
- [29] Sean A Hayward. Formation and evaporation of nonsingular black holes. *Physical review letters*, 96(3):031103, 2006.
- [30] Caio FB Macedo and Luís CB Crispino. Absorption of planar massless scalar waves by bardeen regular black holes. *Physical Review D*, 90(6):064001, 2014.
- [31] Caio FB Macedo, Ednilton S de Oliveira, and Luís CB Crispino. Scattering by regular black holes: planar massless scalar waves impinging upon a bardeen black hole. *Physical Review D*, 92(2):024012, 2015.
- [32] Valeri P Frolov. Notes on nonsingular models of black holes. *Physical Review D*, 94(10):104056, 2016.
- [33] Sebastian Murk and Ioannis Soranidis. Regular black holes and the first law of black hole mechanics. *Physical Review D*, 108(4):044002, 2023.
- [34] Zhijun Song, Huajie Gong, Hai-Li Li, Guoyang Fu, Li-Gang Zhu, and Jian-Pin Wu. Quasinormal modes and ringdown waveforms of a frolov black hole. *Communications in Theoretical Physics*, 76(10):105401,

2024.

- [35] Shubham Kala, Hemwati Nandan, Kush Maithani, Saswati Roy, and Amare Abebe. Null geodesics, thermodynamics, weak gravitational lensing, and black hole shadow characteristics of a frolov regular black hole with constraints from eht observations. *The European Physical Journal Plus*, 140:991, 2025.
- [36] Subrahmanyam Chandrasekhar. *The mathematical theory of black holes*, volume 69. Oxford university press, 1998.
- [37] Yang Li and Yan-Gang Miao. Absorption cross section of regular black holes in scalar-tensor conformal gravity. *Physical Review D*, 105(4):044031, 2022.
- [38] Yang Huang, Dao-Jun Liu, and Hongsheng Zhang. Dynamics of photons and shadows for black holes haired with parity-odd fields. *Journal of High Energy Physics*, 2025(11):1–18, 2025.
- [39] Kun Meng, Xi-Long Fan, Song Li, Wen-Biao Han, and Hongsheng Zhang. Dynamics of null particles and shadow for general rotating black hole. *Journal of High Energy Physics*, 2023(11):1–28, 2023.
- [40] Yang Huang, Dao-Jun Liu, and Hongsheng Zhang. Lensing and light rings of parity-odd rotating boson stars. *Science China Physics, Mechanics & Astronomy*, 68(8):280411, 2025.
- [41] Robert M. Wald. *General Relativity*. University of Chicago Press, Chicago, 1984.
- [42] Vitor Cardoso, Alex S Miranda, Emanuele Berti, Helvi Witek, and Vilson T Zanchin. Geodesic stability, lyapunov exponents, and quasinormal modes. *Physical Review DParticles, Fields, Gravitation, and Cosmology*, 79(6):064016, 2009.
- [43] Marco AA de Paula, Luiz Leite, and Luís CB Crispino. Geodesic analysis, absorption and scattering in the static hayward spacetime. *arXiv preprint arXiv:2311.15771*, 2023.
- [44] Richard A Matzner, Cécile DeWitte-Morette, Bruce Nelson, and Tian-Rong Zhang. Glory scattering by black holes. *Physical Review D*, 31(8):1869, 1985.
- [45] Marco AA de Paula, Luiz Leite, and Luís CB Crispino. Scattering properties of charged black holes in nonlinear and maxwells electrodynamics. *The European Physical Journal Plus*, 137(7):1–13, 2022.
- [46] DR Yennie, D_ G_ Ravenhall, and RN Wilson. Phase-shift calculation of high-energy electron scattering. *Physical Review*, 95(2):500, 1954.
- [47] Sam Dolan, Chris Doran, and Anthony Lasenby. Fermion scattering by a schwarzschild black hole. *Physical Review DParticles, Fields, Gravitation, and Cosmology*, 74(6):064005, 2006.
- [48] Zhao Li and Wen Zhao. Rigorous calculation of scalar scattering in the schwarzschild background: The convergence of the partial-wave series and the poisson spot. *Physical Review D*, 112(8):083030, 2025.
- [49] Marco AA Paula, Luiz CS Leite, and Luis CB Crispino. Electrically charged black holes in linear and nonlinear electrodynamics: Geodesic analysis and scalar absorption. *Physical Review D*, 102(10):104033, 2020.
- [50] Qian Li, Qianchuan Wang, and Junji Jia. Absorption and scattering of charged scalar waves by charged horndeski black hole. *Physical Review D*, 111(2):024059, 2025.
- [51] Qian Li, Qianchuan Wang, and Junji Jia. Scattering of charged massive scalar waves by kerr-newman black holes. *arXiv preprint arXiv:2511.21318*, 2025.

[52] Zhao Li, Shaoqi Hou, and Wen Zhao. Gravitational lensing of gravitational waves: Spin-wave optics through black hole scattering. *arXiv preprint arXiv:2512.23933*, 2025.